GABA Neurons in the Amygdala play a central Role in Urocortin-3–Mediated Stress Suppression of Reproduction

Author Information

Junru Yu,[1,†] Saeed Farjami,[2,3,†] Kateryna Nechyporenko,[2,3,†] Xiao Feng Li,[1] Hafsa Yaseen,[1,4] Yanyan Lin,[1] Jinbin Ye,[1] Owen Hollings,[1] Ross de Burgh,[1] Baban Singh,[1] Kevin T. O'Byrne,[1,*] Krasimira Tsaneva-Atanasova,[2,3,5,*] Margaritis Voliotis[2,3,*]

Affiliations

[1]Department of Women and Children's Health, School of Life Course and Population Sciences, King's College London, Guy's Campus, London SE1 1UL, UK, [2]Department of Mathematics and Statistics, [3]Living Systems Institute, [4]Biological Sciences, University of Missouri, Columbia, MO 65211-7400 and [5]EPSRC Hub for Quantitative Modelling in Healthcare, University of Exeter, Stocker Road, Exeter EX4 4PY, UK

Abstract

Stress can disrupt menstrual cycles, cause infertility, and lead to other reproductive disorders. The posterodorsal medial amygdala (MePD) processes stress signals and regulates the gonadotropin-releasing hormone (GnRH) pulse generator through GABAergic inhibitory projections to the hypothalamus. However, how stress is processed in the MePD - especially involving its dense GABA and Urocortin-3 (UCN3) neurons - remains poorly understood.

In this study, we combine *in vivo* GRadient-INdex (GRIN) lens mini-endoscopic calcium imaging (to track neuronal activity), optogenetics, clustering analysis, and computational modeling to investigate MePD circuitry. Our findings reveal two anti-correlated GABA sub-populations in the MePD that dictate responses to both UCN3 neuron stimulation and restraint stress. Our computational modeling suggests that mutual inhibition between these GABA groups drives this anti-correlated activity and predicts how these interactions shape downstream responses to stimulation of GABA and UCN3 neurons.

We test these predictions using optogenetics and confirm that GABA neurons are critical for the transmission of UCN3 signals to regulate luteinizing hormone (LH) pulse frequency. Our study is the first to show how GABA neurons in the amygdala mediate stress effects on reproductive health, uncovering key neural mechanisms linking emotional and reproductive functions.

32 ## Introduction

33 Successful reproduction requires normal function of a neural oscillator, the gonadotropin-releasing
34 hormone (GnRH) pulse generator, that drives the pulsatile release of gonadotropic hormones,
35 luteinizing hormone (LH) and follicle stimulating hormone (FSH) to control ovulation and
36 spermatogenesis. This oscillator comprises Kisspeptin neurons co-expressing Neurokinin-B (NKB)
37 and Dynorphin A (acronym KNDy) in the hypothalamic arcuate nucleus (ARC). The KNDy neural
38 network not only provides the essential episodic stimulatory kisspeptin signal to the GnRH neurons,
39 but receives diverse afferent inputs and hence is a hub for integrating various internal and external
40 cues that regulates reproductive function[1,2]. Despite the marked heterogeneity of the myriad
41 stressors, including acute versus chronic experimental stress paradigms, the common denominator
42 is suppression of GnRH pulse generator frequency, which is associated with stress-related
43 reproductive disorders and infertility [3–8].

44 The amygdala, a part of the limbic brain typically associated with emotions and anxiety, has strong
45 projections to the KNDy system[1,2]. The medial amygdala, and more specifically its posterodorsal
46 subnucleus (MePD), has been shown to be a robust upstream regulator of GnRH pulse generator
47 frequency[9–11], pubertal timing[12,13], sociosexual behaviour[14,15], anxiety[14] and psychological stress-
48 induced suppression of pulsatile LH secretion[16,17].

49 In the MePD, the majority of neurons are GABAergic, accounting for a substantial portion of its
50 projections, many of which target important hypothalamic centers involved in reproduction[18–20],
51 including the KNDy neurons and optogenetic stimulation of the latter suppress LH pulsatility[17].
52 Moreover, chemogenetic inhibition of GABA neurons in the MePD can reverse the inhibitory effect of
53 psychogenic stress on LH pulsatility[17], suggesting an involvement of GABA signaling in the stress-
54 induced suppression of pulsatile LH secretion. Although the precise way in which the MePD GABA
55 neurons influence LH pulsatility is not fully understood, it has been suggested that they interact with

56 the stress neuropeptide urocortin-3 (UCN3) neurons to modulate or reinforce stress-induced
57 suppression of LH pulse frequency[16].

58 UCN3, part of the corticotropin-releasing factor (CRF) superfamily and selective for CRF type 2
59 receptors (CRFR2)[21], is highly expressed in the MePD[16,22]. Furthermore, UCN3 neurons in the
60 MePD mediate psychosocial stress-induced suppression of the GnRH pulse generator and
61 corticosterone secretion, thus play a central role in the interaction between the reproductive and
62 stress axes[16,23]. Previously we have shown that intra-MePD GABA antagonism can reverse UCN3-
63 induced LH pulse suppression[23], suggesting that GABA acts downstream of UCN3 signalling within
64 the MePD. However, the local neural circuitry within the MePD mediating stress related information
65 to the GnRH pulse generator remains to be established.

66 Here, we employed GRadient INdex (GRIN) lens mini-endoscopy to monitor and compare the
67 calcium activity of GABA neurons at single-cell resolution under acute psychological stress or
68 optogenetic stimulation of UCN3 neurons. Clustering analysis of the observed calcium transients
69 uncovered two distinct GABA sub-populations exhibiting anti-correlated activity. To explore the
70 functional role of these two sub-populations and unpick the mechanisms driving their anti-correlated
71 activity, we build upon our previously developed MePD circuitry mathematical modeling framework[11].
72 Our modeling reveals that mutual inhibitory interactions between the GABA populations are sufficient
73 to drive anti-correlated activity and predicts a complementary inhibitory effect of GABA and UCN3
74 signaling on the frequency of the GnRH pulse generator, which we tested by applying Cre/Flp
75 recombinase intersectional strategies to selectively target and manipulate heterogeneous MePD
76 neuronal populations[17]. Hence, by uncovering precise interactions between distinct sub-populations
77 of MePD GABA neurons and UCN3 neurons in transmitting stress signals to the GnRH pulse
78 generator, we provide critical and previously unknown insights into the neural circuitry driving stress-
79 induced reproductive dysfunction. This discovery significantly advances our understanding of how
80 emotional stress directly impacts reproductive health and identifies potential neural targets for
81 therapeutic intervention in stress-related reproductive disorders.

Results

Dynamic reconfiguration of MePD GABA neuronal networks during selective optogenetic stimulation of urocortin-3 (UCN3) neurons and restraint stress

To investigate how the posterodorsal subnucleus of the medial amygdala (MePD) processes stress signals and to understand the role of GABA and UCN3 neurons in this process, we employed *in vivo* calcium imaging using GRadient INdex (GRIN) mini-endoscopy. A cohort of six female UCN3-Cre::VGAT-Flpo transgenic mice were injected with a viral mixture containing pAAV-Syn-Flex-rc[Chrimson-tdTomato] and pAAV-EF1a-fDIO-GCaMP6s. This intersectional viral strategy enabled dual functionality: (i) optogenetically stimulating MePD UCN3 neurons via Chrimson; and (ii) detecting calcium activity in MePD GABA neurons using GCaMP6s (Fig. 1**A**). GRIN lenses were surgically implanted at the same location as the viral injection, enabling imaging of calcium activity with single-neuron resolution (Fig. 1**B-G**). The specificity of the AAV-Syn-Flex-rc[Chrimson-tdTomato] expression in the MePD was quantified by overlapping analysis with the UCN3 immunohistochemical staining and revealed that 95.06 ± 2.24% of tdTomato-positive neurons co-localized with the UCN3 immunohistochemical positive neurons (Supplementary Fig. 1). Further, 81.61 ± 6.03% of the total UCN3-immunoreactive neurons co-expressed Chrimson-tdTomato (Supplementary Fig. 1).

Two series of experiments were conducted to assess GABAergic responses under distinct conditions. First, to assess the role of UCN3 neurons in recruiting GABAergic response, baseline calcium activity from MePD GABA neurons was recorded for 2 min, followed by 2 min of recording during optogenetic stimulation of UCN3 neurons (Fig. 1**A**). Optogenetic stimulation was delivered in a discontinuous pattern, 5 seconds on, 5 seconds off, with a light-pulse frequency of 10 Hz during the ‘on’ periods (10-ms pulse width, 10 mW power, and 532 nm wavelength). GABA neurons with activity that mimics the pattern of optic stimulation, evidence that they are co-expressing UCN3, are removed from further analysis (see Methods and Supplementary Fig. 2). To further characterize the GABAergic response to acute stressors, baseline calcium activity of GABA neurons was recorded for 2 min, followed by 2 min of recording while the animals were exposed to restraint stress (Fig.

109 1**A**). The dynamic GABAergic response to optogenetic stimulation of UCN3 neurons and restraint
110 stress was summarized in functional terms using pairwise (neuron-neuron) association matrices,
111 constructed from Pearson correlation coefficients between neuronal trace pairs (see Methods).
112 These correlation matrices represent the MePD GABAergic response as a graph of interconnected
113 nodes (neurons) with edge weights corresponding to the strength of their pairwise functional
114 interactions (Fig. 1**H**&**I**)[24]. To quantify the effect of stress or UCN3 activation on functional
115 connectivity we calculated the normalized Riemannian distance between the correlation matrices
116 from baseline and stimulation/stress periods. Our analysis revealed significant alterations in the
117 functional connectivity of the GABAergic network during both UCN3 stimulation and stress relative
118 to control animals lacking channelrhodopsin expression (Fig. 1**J**). Furthermore, on average, stress
119 induces a significant increase in the population's time-averaged calcium activity in contrast to UCN3
120 stimulation; however, this effect diminishes over the 2-minute stress period (Fig. 1K). These results
121 indicate that the GABA population in the MePD plays a pivotal role in processing stress signals,
122 such as those induced by restraint stress. Furthermore, our findings suggest that UCN3 neurons
123 may serve as a key relay, driving functional reorganization within the GABAergic population to
124 support the transmission of stress-related information.

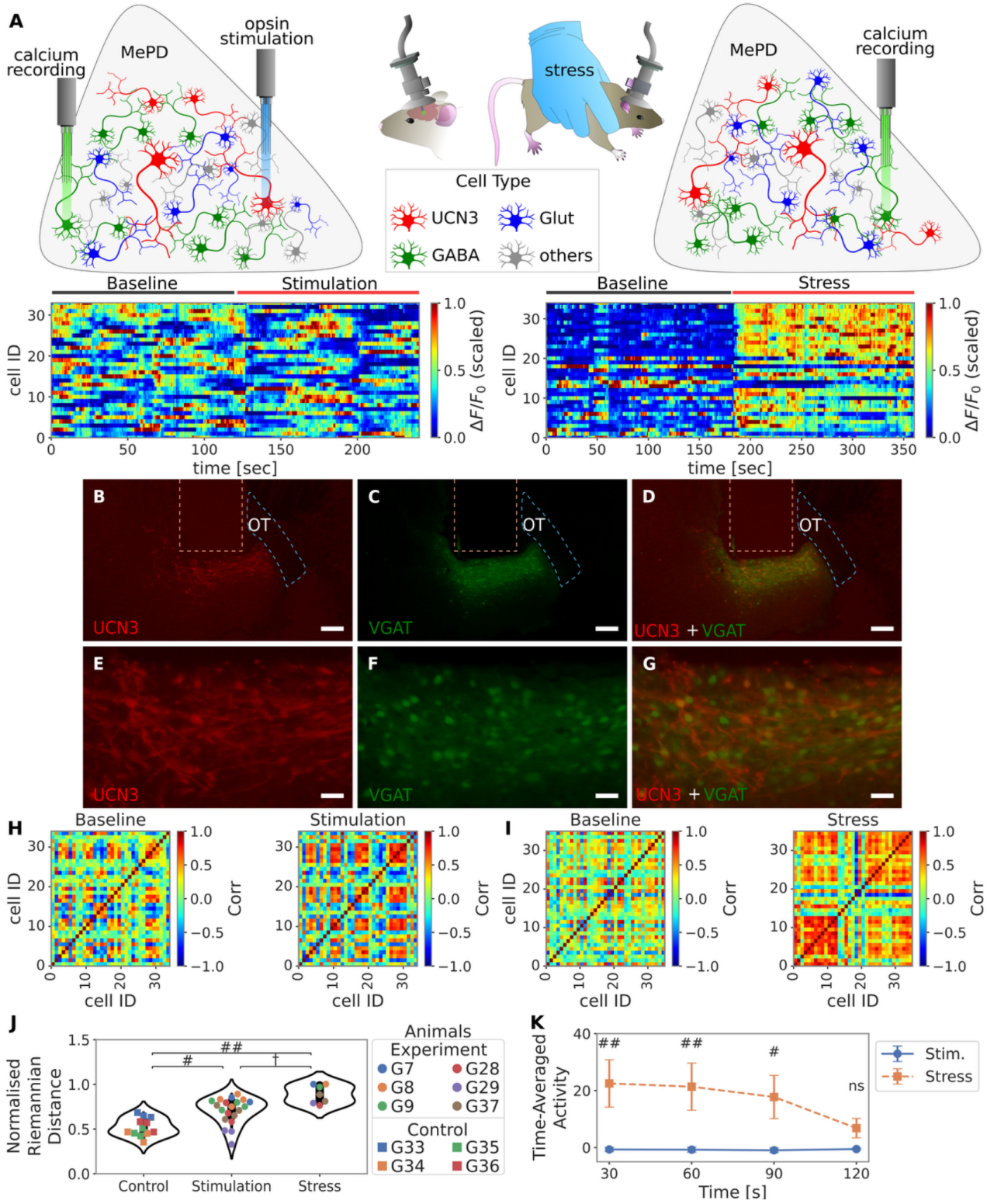

Figure 1: Functional connectivity of GABA neurons in posterodorsal medial amygdala (MePD) reconfigures in response to optogenetic stimulation of urocortin-3 (UCN3) neurons or acute restraint stress. (A) Schematic diagram of the experimental design for stimulating MePD UCN3 neurons and simultaneously imaging calcium activity from MePD GABA neurons. Heatmaps of calcium activity (ΔF/F) (left) in response to optogenetic stimulation of UCN3 neurons excluding GABA cells co-expressing UCN3 (see

131 Supplementary Fig. 2) and (right) during restraint-induced stress. **(B-G)** Representative photomicrographs of
132 the MePD from a UCN3-Cre::VGAT-Flpo mouse injected with pAAV-Syn-Flex-rc+pAAV-EF1a-fDIO-
133 GCaMP6s. **(B&E)** Red fluorescence (tdTomoato) labels UCN3 neurons expressing Chrimson-tdTomato,
134 **(C&F)** green fluorescence labels GABA neurons, and (D&G) red and green signals merged. **(H&I)** Functional
135 connectivity matrices during baseline and under UCN3 activation and stress were constructed by calculating
136 the pairwise Pearson's correlation between calcium time-traces. **(J)** Normalized Riemannian distance between
137 the correlation matrices from baseline and stimulation/stress periods. Each data point represents a single
138 experiment, with different animals color-coded; control animals are shown as squares, and channelrhodopsin-
139 expressing animals as circles. (**K**) Difference in time-averaged calcium activity between periods of UCN3
140 stimulation or stress and the baseline period. Scale bars: **B**-**D**, 200 μm; **E**-**G**, 50 μm.

141 **Clustering analysis reveals two functionally distinct GABA sub-populations in the MePD**

142 To better understand the functional organization of the GABA MePD network during optogenetic
143 stimulation of UCN3 neurons and under restraint stress, we performed clustering analysis on the
144 functional connectivity atrices we obtained from the calcium recordings of GABA neurons.

145 Clustering results consistently revealed two functionally distinct cell populations both during
146 optogenetic stimulation of UCN3 neurons and restraint stress (Fig. 2**A**&**C**). Under both conditions,
147 activity between the two clusters appeared highly anti-correlated as illustrated by two representative
148 examples depicted in Fig. 2**B**&**D**. Moreover, we find that clusters are significantly different in size
149 with the smallest cluster accounting on average for 35% of all cells (Fig 2E&F, Supplementary Fig.
150 3). The robustness of the above finding was also verified using the K-means clustering algorithm
151 and an alternative measure of association between neuronal traces that accounts for time-lag and
152 sign in neuronal interactions (see Methods and Supplementary Figs. 4-6).

153 Varying the frequency of optogenetic stimulation of UCN3 neurons influenced the functional
154 connectivity within the GABA network (Supplementary Fig. 7). Stimulation at 5 Hz produced no
155 significant change compared with controls, 10 Hz resulted in a statistically significant increase, while
156 20 Hz reduced the effect, consistent with a depolarization block. In contrast, stimulation at 5, 10, or
157 20 Hz did not significantly affect the correlation between the average activity of the two GABA

158 clusters (Supplementary Fig. 8). Based on the functional role of the MePD in relaying stress signals
159 to the hypothalamic arcuate nucleus (ARC), our results suggest that the identified GABA sub-
160 populations (clusters) could correspond to distinct populations of GABA interneurons and GABA
161 efferent neurons—defined as neurons that transmit signals from the MePD to downstream targets.
162 Known efferent projections to ARC play a role in regulating the gonadotropin-releasing hormone
163 (GnRH) pulse generator, a key driver of reproductive function[11,17].

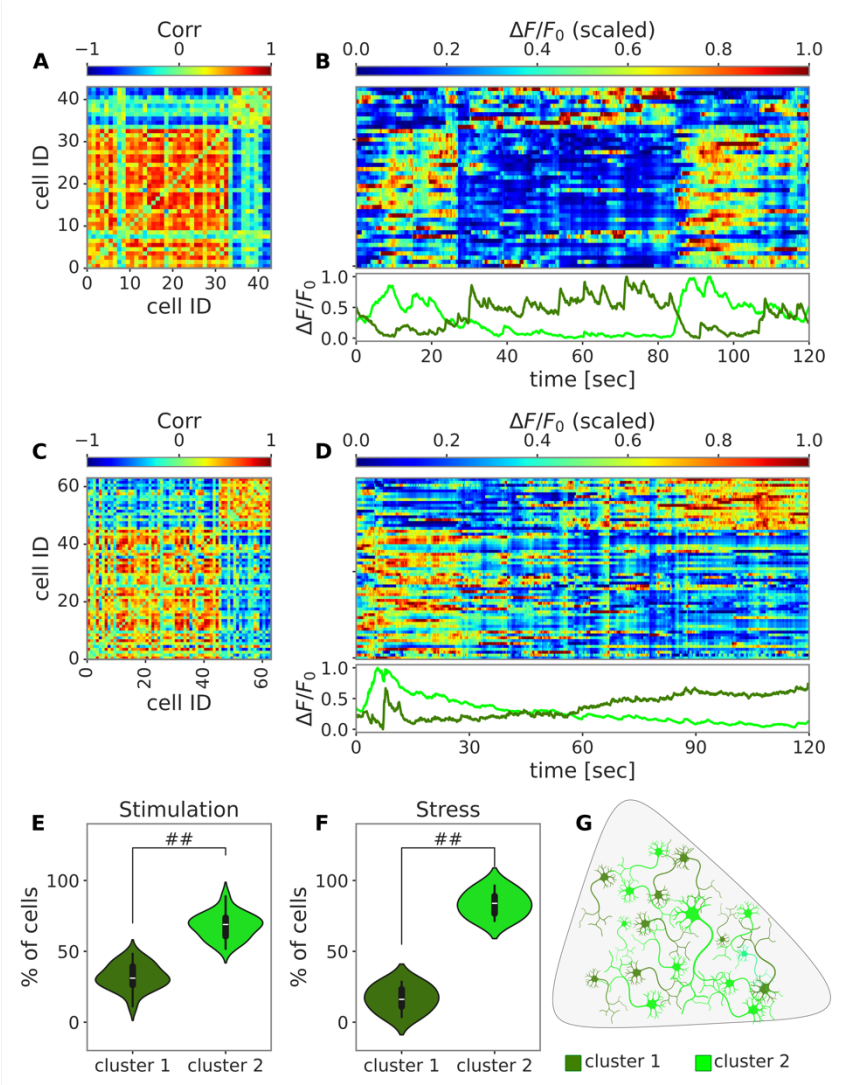

164

165 **Figure 2**: **Clustering identifies two functionally distinct GABA sub-populations in the posterodorsal**
166 **medial amygdala (MePD) both during UCN3 optogenetic stimulation and restraint stress**.
167 Representative example of (**A**) a clustered connectivity matrix and (**B**) associated calcium time-traces of
168 MePD GABA neurons during optogenetic stimulation of UNC3 neurons. Representative examples of (**C**) a
169 clustered connectivity matrix and (**D**) associated calcium activity time-traces of MePD GABA neurons during

170 restraint stress. (**E**&**G)** Relative sizes of the two GABA sub-populations identified via clustering analysis. (##:
171 p<0.001).

172 **Mutually inhibitory interactions between GABA populations drive anti-correlated activity**

173 To explore the network mechanisms driving the anticorrelated activity of the GABA sub-populations,
174 we build upon our previously developed MePD circuit model[11]. The model allows us to explore
175 interactions between MePD neuronal populations and understand emergent patterns of dynamical
176 activity. Specifically, the model describes the calcium dynamics of two interacting populations of
177 GABA neurons, corresponding to interneurons and efferent projection neurons. Efferent neurons
178 project their axons outside the MePD to downstream targets such as the KNDy network. Both GABA
179 populations interact with a glutamatergic population (Fig. 3**A**). Experimental evidence shows that
180 antagonizing glutamate signaling completely blocks the suppressive effect of MePD UCN3
181 activation on LH pulsatility[23], highlighting a functional role of glutamatergic neurons in the circuit.
182 Therefore, the activity of the glutamatergic population is also included in the MePD model alongside
183 the two GABA populations. Model equations are provided in Supplementary Information, and the
184 parameter values for the MePD model are in Supplementary Tab. 1.

185 To incorporate UCN3 input we include a non-autonomous term in the model informed by recordings
186 of the activity of UCN3 neurons during optogenetic stimulation (see Fig. 3**A** and Methods). The
187 recorded traces exhibit a periodic pattern driven by the experimental stimulation protocol with 5
188 seconds on, 5 seconds off (see Methods). In the model, we approximated this UCN3 input using a
189 sinusoidal function with roughly 5 seconds on, 5 seconds off pattern, driving the populations GABA
190 interneurons and the glutamatergic neurons. To reproduce the anti-correlated activity between the
191 two GABA neuronal sub-populations while also reproducing previously published results on the
192 effects of neuropharmacological perturbations in the MePD on LH pulsatility[23], we find that we need
193 to include bi-directional (i.e. mutually inhibitory) GABA interaction in the circuit as well as GABA
194 interneurons self-inhibition (Fig. 3**A**).

Next, we validate our model by simulating the effects of stress on the MePD circuit. UCN3 neurons in the MePD have also been shown to mediate psychosocial stress-induced suppression of the GnRH pulse generator[16]. Experimentally recorded calcium activity of UCN3 neurons during stress intervention is characterized by a fast rise followed by a slow decay (Fig. 3**B**), which we model by taking the difference between two exponential functions, one with a fast and one with a slow time constant (see Methods). Using this input, our mathematical model confirms the emergence of anti-correlated behavior between the GABA sub-population whereby the activity of GABA interneurons decreases over the stress period, while the activity of the GABA efferent neuron population increases (Fig. 3**B**), supporting the proposed MePD circuit structure (Fig. 3**A**).

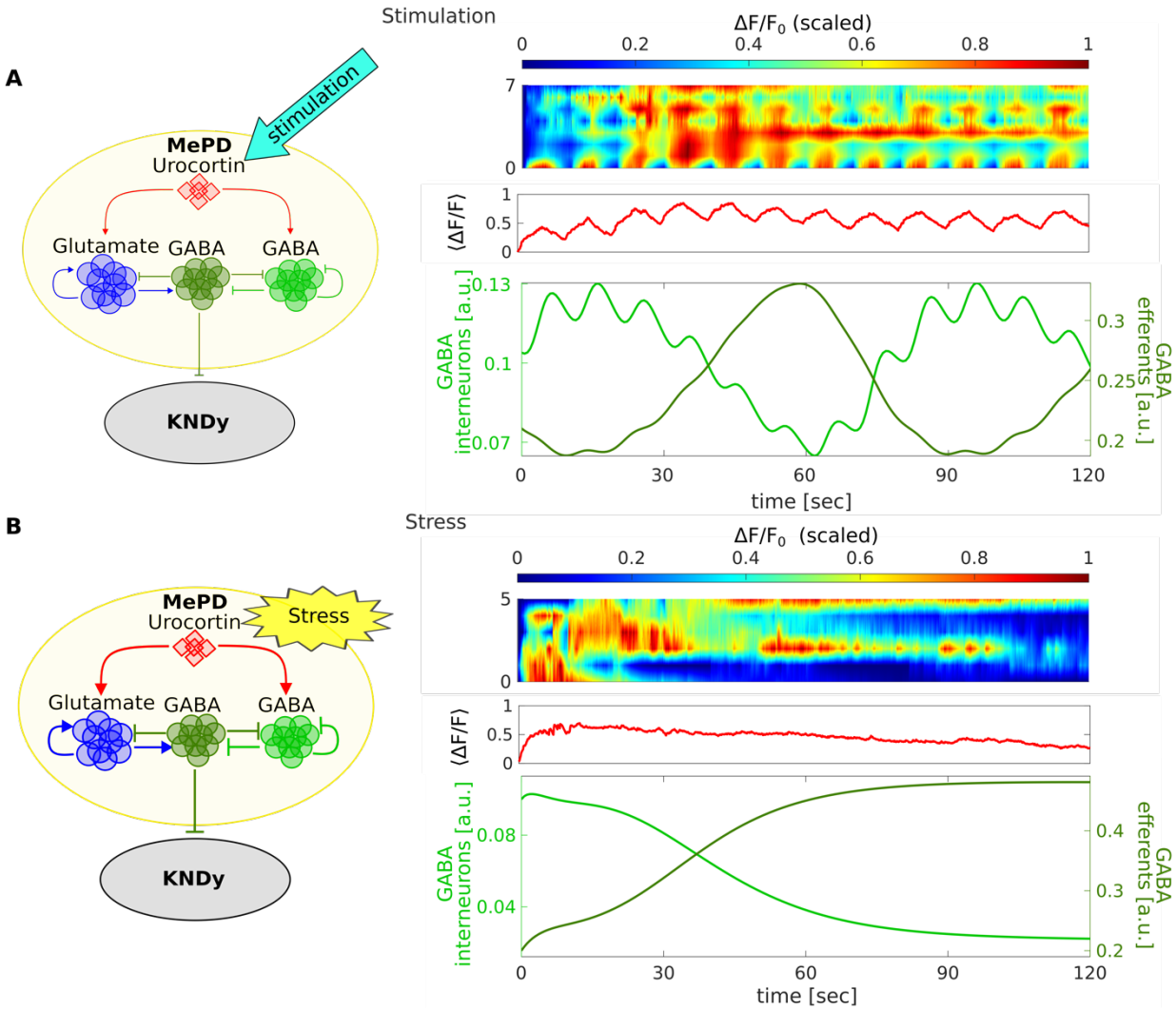

Figure 3: *In silico* simulation of the activity in the GABA neuronal populations in the MePD under the increased excitatory input from UCN3 neurons and under restraint stress. Schematic on the left

207 represents the MePD neuronal circuit interacting with UCN3, consisting of two GABA populations and a
208 glutamatergic population. **(A)** Calcium time-traces of MePD UCN3 neurons during optogenetic stimulation of
209 UCN3 neurons and corresponding mean activity. Model simulations of the effects of UCN3 optogenetic
210 stimulation supports the emergence of anti-correlated activity in GABA sub-populations. **(B)** Calcium time-
211 traces of MePD UCN3 neurons during restraint stress and corresponding mean activity of the UCN3 calcium
212 traces during restraint stress with corresponding mean activity. Simulations of the MePD circuit under the
213 effects of stress also support anti-correlated GABA sub-populations' activity.

214 ***In silico* modeling reveals complementary relationship between MePD GABA and UCN3**
215 **populations**

216 Having shown that MePD model can reproduce anti-correlated activity of two GABA sub-
217 populations, we examine the effects of distinct interventions involving GABA and UCN3 in the MePD
218 on the LH pulses. To do that we couple the model of the MePD circuitry defined in the previous
219 section to our network model of the KNDy population in the arcuate nucleus (ARC)[11,25]. KNDy model
220 details are in Supplementary Information and the model parameter values can be found in
221 Supplementary Tab. 2. Since KNDy neuronal activity serves as a well-established proxy for LH
222 secretion, we use the dynamics of the KNDy network model to infer changes in LH pulsatility in
223 response to MePD circuit manipulations. Our previous in silico findings[11] show that MePD signal
224 integration is predominately mediated by GABA projections. The effects of MePD GABA and
225 glutamate antagonism alone and together with UCN3 stimulation on LH pulsatility have been
226 previously investigated[23], and we use these experimental findings to calibrate our coupled model
227 parameters by reproducing these effects accordingly (see Supplementary Fig. 9).
228 Next, using the calibrated model, we predict that providing a periodic excitatory input (see
229 Supplementary Fig. 10(A)), that mimics the effects of optogenetic stimulation of UCN3, leads to the
230 increase in the KNDy inter-pulse interval (IPI) from 15.18 min to 23.97 min due to increased activity
231 in the inhibitory GABAergic input to the KNDy network (Fig. 4A).
232 Since MePD has an overwhelming number of GABAergic outputs and interneurons, we are
233 interested in their role in information processing of stress signaling. To this end we provide periodic

234 excitatory input directly to both populations of GABA neurons (see Methods and Supplementary
235 Information). This is different to the indirect activation through UCN3 stimulation, as it leads to the
236 increased activity in both GABA subpopulations (Supplementary Fig. 10(B)). The resulting effect on
237 the KNDy IPI is an increase from 15.18 min to 42.65 min (Fig. 4B).
238 In the model we hypothesize that UCN3 signaling to the KNDy is operating through the GABAergic
239 pathway, hence disrupting GABAergic interactions will suppress UCN3's effects on KNDy. To
240 investigate it we suppress the strength of the GABAergic interactions by 50% and mimic UCN3
241 stimulation by providing excitatory input to the circuit. The model shows that this intervention does
242 not have a significant effect on KNDy IPI, apart from slightly increasing it from 15.18 min to 17.31
243 min (Fig. 4C & Supplementary Fig. 10(C)).
244 Taken together the above could be summarized as the following set of model predictions along with
245 suggested ways to test them experimentally:

246 1. Optogenetic stimulation modelled via excitation of the MePD UCN3 increases the KNDy IPI
247 15.18 min to 23.97 min. This could be tested experimentally via in vivo optogenetic activation
248 of the MePD UCN3 neuronal populations and simultaneous measurement of LH pulsatility.
249 2. Stimulation of the MePD GABA populations increases the KNDy IPI 15.18 min to 42.65 min.
250 Such a substantial change underscores the critical role of GABAergic signaling in modulating
251 KNDy pulsatility. Experimental confirmation could involve in vivo optogenetic activation of the
252 entire MePD GABA population accompanied by LH pulsatility measurement.
253 3. Stimulation of the MePD UCN3 with simultaneous suppression of the GABAergic interactions
254 in the MePD does not significantly affect KNDy IPI, changing it from 15.18 min to 17.31 min.
255 This finding suggests that UCN3 effects on the KNDy network are primarily dependent on its
256 interactions with GABA populations. A strategy to verify this hypothesis experimentally could
257 be to stimulate UCN3 non-GABA-expressing neurons in vivo while simultaneously inhibiting
258 non-UCN3 GABA neurons and measure LH pulsatility.

259 Finally, we investigate in silico the effects of stress on LH pulse dynamics mediated via the MePD.
260 In the restraint-stress experiment it was shown that one GABA cluster was active, while the other

261 one was inactive (Fig. 2D). By simulating these dynamics (Supplementary Fig. 9(D)) in the coupled
262 MePD - KNDy network model we are able to demonstrate that pulses in the KNDy network ceased
263 (Fig. 4D). These modeling findings align with published experimental evidence indicating that
264 restraint stress suppresses LH pulsatility[16].

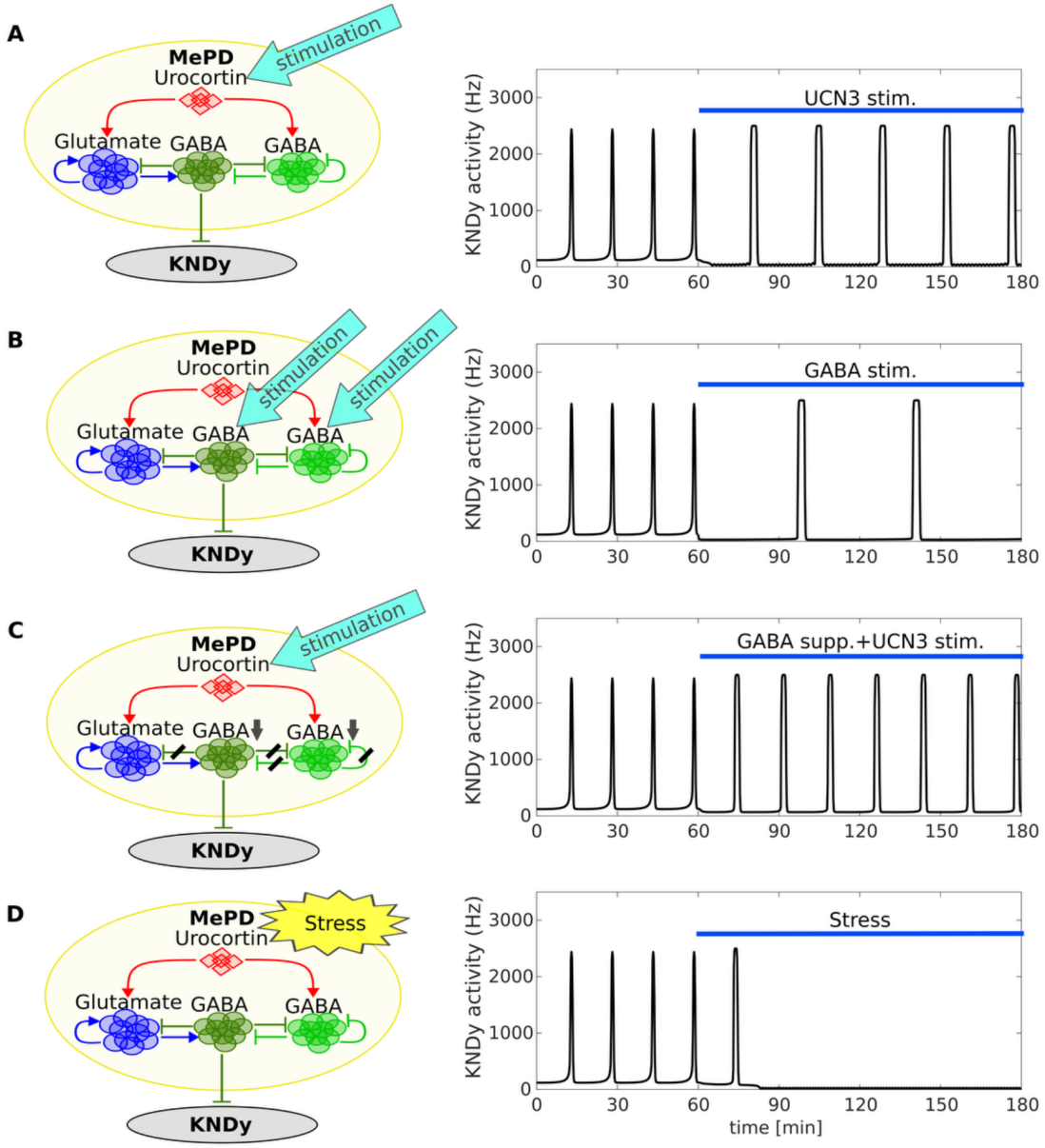

265

266 **Figure 4: Coupled MePD - KNDy model predictions for the effect of stress and stimulation of UCN3**
267 **neurons on GnRH pulse generator activity and hence LH pulsatility.** (A) Simulation of the optogenetic
268 stimulation of the UCN3 neurons leads to the increase of the KNDy IPI 15.18 min to 23.97 min. (B)
269 Optogenetic stimulation of the MePD GABA neurons (providing excitatory input to both GABA populations)

270 increases KNDy IPI from 15.18 min to 42.65 min. (C) Optogenetic stimulation of the UCN3 neurons and
271 simultaneous inhibition of GABA neuronal populations do not significantly affect KNDy IPI, where it changes
272 from 15.18 min to 17.32 min. (D) Simulating the effects of stress leads to the cessation of the pulsatile
273 dynamics.

274 **Selective optogenetic stimulation of UCN3 non-GABA neurons inhibits pulsatile LH secretion**
275 **in female mice.**

276 We now test experimentally our modeling predictions detailed in the previous section regarding the
277 inhibitory effect of MePD UCN3 activation on LH pulsatility in vivo in freely behaving mice. To this
278 end a cohort of UCN3-Cre::VGAT-Flpo transgenic female mice was injected with an AAV-nEF-
279 Con/Foff 2.0-ChRmine-oScarlet viral construct. This intersectional approach enabled conditional
280 expression of channelrhodopsin (ChRmine) in UCN3 neurons not expressing GABA (UCN3 non-
281 GABA) (Con/Foff group). Following the viral injection, a unilateral fiber-optic cannula was implanted
282 into the MePD, above the injection site, to facilitate selective activation of the targeted neuronal
283 population. The specificity of the AAV-nEF-Con/Foff 2.0-ChRmine-oScarlet expression in the MePD
284 was quantified by overlapping analysis with the UCN3 immunohistochemical staining and revealed
285 that 98.92 ± 1.08% of the oScarlet-positive neurons co-localized with the UCN3
286 immunohistochemical positive neurons (Supplementary Fig. 11). Further, 54.18 ± 5.04% of the total
287 UCN3-positive neurons co-expressed ChRmine-oScarlet (Supplementary Fig. 11).

288 The stimulation protocol consisted of a 60-min control period, followed by 60 min of optogenetic
289 stimulation. Stimulation was delivered, as above, in a pulsed pattern (5 seconds on, 5 seconds off)
290 with a pulse frequency of 10 Hz during the on period (10-ms pulse width, 10 mW power, 532 nm
291 wavelength). Blood samples (5 μL) were collected every 5 min throughout the protocol and used to
292 measure LH levels.

293 Statistical analysis indicated post-stimulation LH inter-pulse intervals differed across the two groups
294 ($F(2, 30) = 15.83$, $P < 0.0001$). In the Con/Foff group, the LH inter-pulse interval significantly
295 increased after optogenetic stimulation compared to the control period (15.47 ± 0.91 min vs. 23.75 ±

296 1.07 min, mean ± SEM, n = 6, p<0.01; Fig. 5A&D), validating the first of our modeling predictions. In
297 contrast, the no-stimulation group, which received the Con/Foff viral construct without optogenetic
298 stimulation, showed no significant changes in LH inter-pulse interval (15.84 ± 0.37 min vs. 16.68 ±
299 0.86 min, n = 6, p > 0.05; Fig. 5B&D). Similarly, in a separate cohort of mice injected with a control
300 virus (DIO-EYFP), optogenetic stimulation resulted in no significant differences in LH inter-pulse
301 intervals before and after stimulation (19.83 ± 1.02 min vs. 17.78 ± 0.93 min, n = 6, p > 0.05; Fig.
302 5C&D). The LH pulse amplitude and mean LH levels were quantified, and data are provided in
303 Supplementary Table 3.

304 **Selective optogenetic stimulation of UCN3-expressing GABA neurons fails to affect pulsatile**
305 **LH secretion in female mice.**

306 To further test the functional interactions between the UCN3 and GABA populations, a separate
307 cohort of UCN3-Cre::VGAT-Flpo transgenic female mice was injected with an AAV-nEF-Con/Fon
308 2.0-ChRmine-oScarlet viral construct, which allows optogenetic stimulation of UCN3 neurons co-
309 expressing GABA (UCN3-expressing GABA) (Con/Fon group). The specificity of the AAV-nEF-
310 Con/Fon 2.0-ChRmine-oScarlet expression in the MePD was quantified by overlapping analysis with
311 the UCN3 immunohistochemical staining and revealed that 98.77 ± 1.24% of the oScarlet-positive
312 neurons co-localized with the UCN3 immunohistochemical positive neurons co-expressing GABA
313 (Supplementary Fig. 12). Further, 32.73± 2.60% of the total UCN3-positive neurons co-expressed
314 ChRmine-oScarlet (Supplementary Fig. 12).

315 Statistical analysis showed no significant interaction effect of group and optogenetic stimulation on
316 LH inter-pulse intervals (two-way ANOVA, F (1, 18) = 0.2709, p = 0.6091). That is, LH inter-pulse
317 intervals in the Con/Fon group, showed no change following optogenetic stimulation compared to
318 the control period (17.92 ± 0.80 min vs. 16.60 ± 0.88 min, mean ± SEM, n = 6, p > 0.05; Fig. 5H&J).
319 Similarly, in the no-stimulation control experiment for this cohort, which did not receive optogenetic
320 stimulation, there was no significant difference in LH inter-pulse intervals (16.08 ± 1.45 min vs.

321 15.83 ± 0.95min, n = 5, p > 0.05; Fig. 5I&J). The LH pulse amplitude and mean LH levels were
322 quantified, and data are provided in Supplementary Table 3.

323 Taken together, our results suggest that both UNC3 and GABA populations relay inhibitory
324 information to the hypothalamic GnRH pulse generator but activation of UCN3 neurons that also co-
325 express GABA is not sufficient.

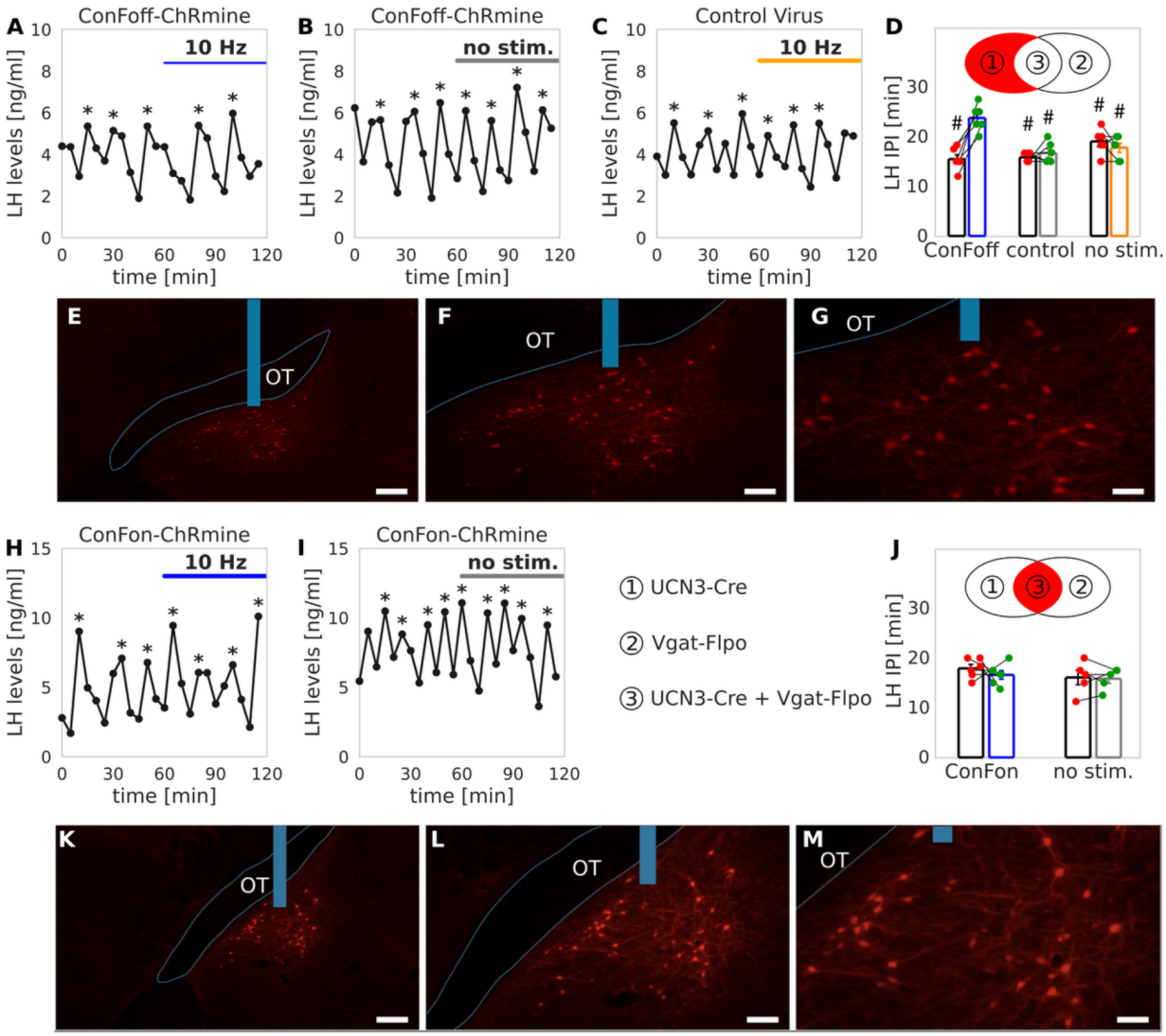

326

327 **Figure 5: Effect of optogenetic stimulation of UCN3 non-GABA and UCN3 neurons co-expressing**
328 **GABA in the MePD on LH pulse frequency.** (A-D) Optogenetic stimulation of UCN3 non-GABA neurons
329 inhibited LH pulses. Representative examples of LH pulsatility in UCN3-Cre::VGAT-Flpo mice injected with
330 AAV-Con/Foff-ChRmine in response to (A) 10Hz optic stimulation or (B) no stimulation as control, and (C) in
331 mice injected with control virus in response to 10 Hz stimulation. Pulses detected by the DynPeak algorithm

332 are indicated with an asterisk (*). (D) Mean LH inter-pulse interval (IPI) (±SEM) for each group during the
333 control period and over the subsequent stimulation period. #: p<0.01 vs stimulation period in Con/Foff group
334 (Two-way ANOVA, Tukey's post-hoc). (E-G) Representative photomicrographs of expression of AAV-nEF-
335 Con/Foff 2.0-ChRmine-oScarlet (red) in MePD UCN3 neurons. (H-M) Optogenetic stimulation of neurons co-
336 expressing UCN3 and GABA in the MePD did not impact LH pulse significantly. Representative examples of
337 LH pulsatility in UCN3-Cre::VGAT-Flpo mice injected with Con/Fon-ChRmine-oScarlet virus in response to (H)
338 10 Hz optic stimulation or (I) no stimulation as control. (J) Mean LH IPI (±SEM) for each group during the
339 control period and over the subsequent stimulation period (Two-way ANOVA). (K-M) Representative
340 photomicrographs of neurons co-expression UCN3 and GABA, tagged with oScarlet (red). Scale bars
341 represent (E&K) 200 μm, (F&L) 100 μm, (G&M) 50 μm. OT, optic track. The blue vertical bars in E to G and K
342 to M indicate the position of the fiber optic cannula.

343 **The MePD GABA neurons relay information from UCN3 neurons and inhibit the GnRH pulse**
344 **generator.**

345 To test our remaining model predictions and establish the functional role of GABA neurons in the
346 MePD in transmitting inhibitory signals to the hypothalamic GnRH pulse generator, we injected the
347 AAV-EF1a-DIO-ChR2-EYFP viral construct into VGAT-Cre transgenic mice, targeting the entire
348 MePD GABA neuron population for expressing ChR2 and used the optogenetic stimulation protocol
349 described above (60 min control period followed by 60 min stimulation) to stimulate the entire MePD
350 GABA population. In the VGAT-Cre-tdtomato mice, we observed that 93.27 ± 2.99% of the EYFP-
351 positive neurons were tdtomato-positive and 87.01± 5.21% of the tdtomato-positive neurons were
352 EYFP-positive. This indicates a high degree of co-expression consistency between the viral and
353 transgenic reporters. Statistical analysis showed a significant interaction effect of our genetic
354 intervention and stimulation period on LH pulsatility ($F(2,24) = 10.55$, $p = 0.0005$; two-way ANOVA).
355 Stimulation of the GABA population markedly increased the LH inter-pulse interval compared to the
356 pre-stimulation control period (18.5 ± 2.03 min vs 49.5 ± 8.46 min, mean ± SEM, n = 5, p<0.01;
357 Tukey's post-hoc; Fig. 6A&D), validating modeling prediction 2. In contrast, mice that did not receive
358 optogenetic stimulation showed no change in LH inter-pulse interval (21.25 ± 3.79 min vs 19.33 ±
359 1.52min, n = 5, p > 0.05; Tukey's post-hoc; Fig. 6**B**&**D**). Similarly, control virus (AAV-EF1a-DIO-

360 EYFP) injections did not result in any significant difference in LH inter-pulse interval before and
361 during stimulation (16.50 ± 0.67 min vs 18.00 ± 0.62min, n = 5, p > 0.05; Tukey's post-hoc; Fig.
362 6**C**&**D**). The LH pulse amplitude and mean LH levels were quantified, and data are provided in
363 Supplementary Table 4

364 Next, UCN3-Cre::VGAT-Flpo transgenic females were injected with an intersectional viral mixture
365 containing AAV-nEF-Con/Foff 2.0-ChRmine-oScarlet and pAAV-nEF-Coff/Fon-NpHR3.3-EYFP ,
366 enabling simultaneous excitation of UCN3 non-GABA neurons and inhibition of non-UCN3 GABA
367 neurons. Statistical analysis showed no significant interaction effect of genetic manipulation and
368 stimulation period on LH pulsatility ($F_{(1, 18)} = 0.131$, $p = 0.7216$; two-way ANOVA). Moreover,
369 optogenetic stimulation resulted in no significant change in the LH inter-pulse interval relative to the
370 control period (16.67 ± 1.31 min vs 18.61 ± 1.58 min, mean ± SEM, n = 6, p > 0.05; Fig. 6**H**&**J**),
371 which aligns with our modeling prediction 3. Similarly, in mice injected with the same viral mixture
372 but without receiving optogenetic stimulation, no significant change in LH inter-pulse interval was
373 detected (16.33 ± 1.19 min vs 17.33 ± 0.81min, n = 5, p > 0.05; Fig. 6**I**&**J**). The LH pulse amplitude
374 and mean LH levels were quantified, and data are provided in Supplementary Table 3.

375 Collectively, these findings suggest that MePD GABA neurons are integral to regulating LH pulse
376 frequency. The inhibitory effect on LH pulses observed upon UCN3 neuron activation is attenuated
377 when GABA neuron activity is optogenetically suppressed, implying that GABA signaling acts
378 downstream of UCN3 neurons, relaying the inhibitory signal to the hypothalamic GnRH pulse
379 generator.

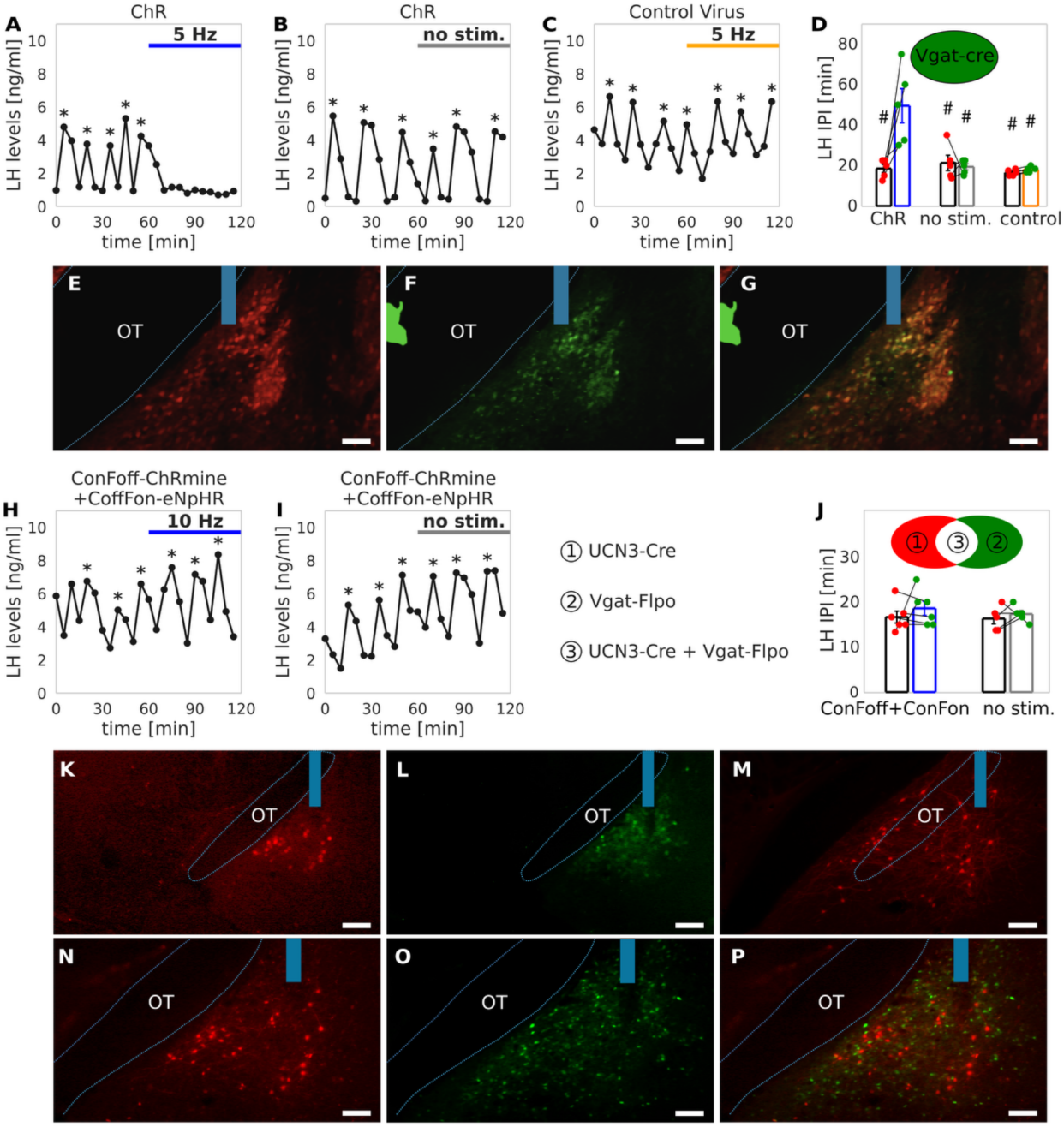

380

381 **Figure 6: Selective optogenetic stimulation of GABA neurons in the MePD inhibits LH pulsatility and**
382 **their activity is necessary for mediating UCN3 signalling downstream.** (**A-G**) Optogenetic activation of
383 the entire MePD GABA population in VGAT-Cre mice led to significant LH pulse suppression. Representative
384 examples showing LH pulsatility in VGAT-Cre mice injected with AAV-double floxed-ChR2-EYFP virus in
385 response to (**A**) 5 Hz stimulation or (**B**) no stimulation as control, and (**C**) 5 Hz stimulation in mice injected with
386 control virus. (**D**) Mean LH IPI (±SEM) for each group during the control period and over the subsequent
387 stimulation period. #: p<0.01, †: p<0.05 vs stimulation period in ChR group (Two-way ANOVA, Tukey's post-

388 hoc). (**E-G**) Representative photomicrographs of MePD GABA neurons, labeled with (**E**) tdTomato (red), (**F**)
389 ChR2-EYFP (green), and (**G**) merged. Scale bars represent. (**H-P**) The simultaneous inhibition of non-UCN3
390 GABA neurons in the MePD restored the LH suppression induced by stimulation of non-GABA UCN3
391 neurons. Representative examples showing LH pulsatility in UCN3-Cre::VGAT-Flpo female mice injected with
392 Con/Foff-ChRmine-oScarlet and Coff/Fon-NpHR-EYFP virus mixture in response to (**H**) 10 Hz optogenetic
393 stimulation or (**I**) no stimulation as control. (**J**) Mean LH IPI (±SEM) for each group during the control period
394 and over the subsequent stimulation period. (Two-way ANOVA). (**K-P**) Representative photomicrographs of
395 fluorescence in MePD neurons. (**K**&**N**) non-GABA UCN3 neurons tagged with oScarlet (red), (**L**&**O**) non-UCN
396 GABA neurons tagged with EYFP (green) (**M**&**P**) merged. Scale bars represent (**E-G**) 150 µm, (**K-M**) 200 µm,
397 (**N-P**) 100 µm. OT, optic track. The blue vertical bars in **E** to **G** and **K** to **P** indicate the position of the fiber
398 optic cannula.

399 Discussion

400 The posterodorsal subnucleus of the Medial Amygdala (MePD), is a critical regulator of reproductive
401 function. Single-cell transcriptomics has revealed a mosaic of glutamatergic and GABA populations
402 in this region, with GABA neurons co-expressing receptors for gonadal steroids as well as
403 neuromodulators and cognate receptors involved in parental and sociosexual behavior (including
404 kisspeptin, prolactin and oxytocin)[26]. Furthermore, calcium imaging of neuronal ensembles from this
405 region have started to decipher how this brain region encodes information about social interactions
406 and stressful stimuli[27], with stress related information being relayed to the reproductive axis via
407 potentially direct projections to the hypothalamus[1,2], and eliciting well-documented responses on
408 pubertal timing[12,13], LH secretion[16,17] and the GnRH pulse generator[9–11]. Here, to elucidate the
409 neuronal circuitry involved in MePD processing of stress signals, we used GRIN lens mini-
410 endoscopic calcium imaging to study, for the first time, the dynamic activity of MePD GABA neurons
411 under acute restraint stress as well as the activity of GABA neurons in response to UCN3 activation.
412 Functional network analysis of the imaging data revealed that acute restraint stress induces a
413 reconfiguration of the GABA population, highlighting their role in encoding and transmitting stress
414 information. Optogenetic stimulation of UCN3 neurons produced a comparable network reconfiguration,

415 despite no significant change in the magnitude of calcium activity compared to baseline, indicating that both
416 populations are co-involved in stress processing. Further clustering analysis of the calcium
417 transients identified two distinct GABA sub-populations with anti-correlated activity. This finding of
418 two distinct populations is consistent with physiological and morphological studies of GABA neurons
419 in the medial amygdala characterizing them as either projecting cells or local interneurons[18,20].

420 Building upon our previously developed computational model of the MePD circuit, we explored the
421 network connectivity to understand the possible mechanisms through which anti-correlated activity
422 emerges. The model consists of a glutamatergic sub-population and two GABA sub-populations:
423 one comprising GABA interneurons and the other GABA efferent projection neurons. Our analysis
424 identified two conditions necessary for the emergence of anti-correlated activity between these
425 GABA sub-populations, consistent with our experimental observations. First, mutual inhibition
426 between the GABA sub-populations is required, such that activation of one population suppresses
427 the other. In our mechanistic model, mutual inhibition arises from the biophysical characteristics of
428 GABAergic transmission, where the release of GABA inhibits target neurons, thereby producing
429 inhibitory interactions between the sub-populations. Second, if both sub-populations receive a
430 shared input (e.g., from the glutamatergic population or any other population of excitatory cells),
431 their dynamics become entrained to that common stimulus, meaning that distinct input streams to
432 each sub-population are necessary for the observed anti-correlation. To satisfy this condition in our
433 model, GABA interneurons receive inputs from UCN3 neurons, whereas the GABA efferent
434 projection neurons receive inputs from the glutamatergic population. This circuitry implies that stress
435 information is processed along two key pathways (one glutamatergic and one GABAergic) and is
436 integrated by the GABA efferent projection neurons.

437 We note that an alternative connectivity pattern, with the UCN3 population directly projecting to the
438 GABA efferent population, could also fit our experimental observations, but does not reproduce
439 previously published results on the effects of neuropharmacological perturbations in the MePD on
440 LH pulsatility[23]. Specifically, the suppression of glutamatergic neurons in combination with
441 stimulation of UCN3 neurons. Under this scenario direct input from stimulated UCN3 to GABA

442 efferent neurons will lead to the increase in its activity, consequently increasing KNDy IPI. This
443 finding contrasts with experimental observations, where the combined suppression of glutamate and
444 stimulation of UCN3 failed to produce any significant change in GnRH pulsatility[23].

445 We note that our MePD model has potential applications beyond understanding MePD dynamics
446 and their influence on the GnRH pulse generator. The model incorporates two functionally distinct
447 populations of GABA neurons (interneurons and efferent projection neurons), which reflect known
448 differences in GABA neurons within the amygdala[18,20]. This diversity likely originates from the medial
449 ganglionic eminence (MGE), an embryonic structure that gives rise to GABA interneuron
450 populations across various brain regions, including the MePD, through migration during
451 embryogenesis[28]. Therefore, the framework of our model could be extended to other neural circuits
452 where two functionally distinct GABA populations exist, such as the posterior ventral medial
453 amygdala[20] and its lateral and basal subdivisions[29].

454 Consistent with model predictions, we showed that optogenetic activation of non-GABA neurons,
455 expressing UCN3, suppresses LH pulse frequency. This finding corroborates previous work
456 demonstrating that LH pulses are inhibited by activation of UCN3 neurons[13,23] or administration of
457 UCN3[16] in the MePD, and that such effects are attenuated by chemogenetic inhibition of UCN3
458 neurons or by antagonizing corticotropin-releasing factor type 2 receptors (CRFR2)[16]. Thus, our
459 findings further support the central role of UCN3 signaling in modulating both stress responses and
460 reproductive function.

461 GABA is one of the primary inhibitory neurotransmitters in the nervous system[18]. Previous work has
462 shown that MePD GABA neurons project to the ARC to regulate LH pulses and chemogenetic
463 inhibition of MePD GABA neurons attenuates stress-induced suppression of LH pulses[17]. In this
464 study, we found that optogenetic activation of GABA neurons in the MePD leads to robust LH pulse
465 suppression, reinforcing the pivotal role of amygdala GABAergic signaling in stress-related
466 reproductive dysfunction. Antagonizing GABA receptors in the MePD can block UCN3-induced LH
467 suppression[23], suggesting that GABA neurons may function downstream of UCN3 signaling.

468 However, this pharmacological approach lacks cell-type specificity, leaving open the possibility that
469 UCN3 neurons themselves co-expressing GABA receptors, potentially contributing to the observed
470 effect. Here, by using an intersectional genetic strategy, we demonstrated that optogenetically
471 inhibiting non-UCN3 GABA neurons can abolish the change in LH pulse intervals induced by
472 optogenetic stimulation of UCN3 neurons. This finding suggests that these GABA neurons may be
473 acting downstream of UCN3 signaling to mediating LH pulse suppression. We note, that while in our
474 current experimental protocol we could also be blocking GABAergic projections to the ARC KNDy
475 population, which by itself could explain the absence of any effect from UCN3 stimulation, our
476 modeling predicts that GABAergic interactions within the MePD are additionally crucial for relaying
477 UCN3 signals to the KNDy network as also suggested by pharmacologically antagonizing GABA
478 receptors[23].

479 It is not unusual for neurons to co-express neuropeptides and neurotransmitters[20]. Given that
480 activating either UCN3 or GABA neurons independently suppresses LH pulses, one might predict
481 that stimulating neurons co-expressing both UCN3 and GABA would similarly inhibit LH. However,
482 we observed no significant changes in LH pulses upon optogenetic stimulation of neurons co-
483 expressing UCN3 and GABA. Our results indicate that UCN3 and GABA are both essential for
484 transmitting inhibitory signals to the hypothalamic GnRH pulse generator; however, this inhibitory
485 influence relies on their action through separate, functionally distinct neuronal populations. That is
486 activation of neurons that exclusively express either UCN3 or GABA suppresses the GnRH pulse
487 generator, whereas activation of UCN3 neurons that also co-express GABA fails to produce this
488 inhibitory effect. Within our modeling framework, UCN3/GABA co-expressing neurons might be
489 considered part of the GABA interneuron population, primarily inhibiting GABA projection neurons
490 rather than activating them. Consequently, they fail to relay the inhibitory UCN3 signal to the ARC.
491 Further studies are necessary to define more precisely the distinct role of UCN3/GABA co-
492 expressing neurons within the MePD circuitry.

493 By combining mini-endoscopic calcium imaging with computational modeling, we identified two
494 GABA sub-populations with complementary but distinct roles in encoding stress signals and

495 modulating LH pulsatility. Our experimental and computational results also stressed the functional
496 orthogonality between UCN3 and GABA signaling in MePD, highlighting the complexity of the
497 MePD's contribution to stress-induced reproductive suppression. These results offer improved
498 understanding of the neuronal circuits in the amygdala, a key hub for emotional processing, involved
499 in regulating hypothalamic GnRH pulse generator frequency[9–11,16,17,23] providing new insight into
500 psychogenic stress-related disorders of fertility, such as functional hypothalamic
501 amenorrhoea[6,7,30,31], and the development of novel therapeutic approaches to improve reproductive
502 health and well-being.

503 **Methods**

504 **Animal**

505 VGAT-Cre-tdTomato mice were genotyped using PCR to determine heterozygosity for VGAT-Cre
506 (primers 5′-3′: common, 12785—CTTCGTCATCGGCGGCATCTG; wild-type reverse12786—
507 CAGGGCGATGTGGAATAGAAA; mutant reverse oIMR8292—CCAAAAGACGGCAATATGGT) and
508 tdtomato (primers 5′-3′: wild-type forward oIMR9020—AAGGGAGCTGCAGTGGAGTA; wild-type
509 reverse oIMR9021—CCGAAAATCTGTGGGAAGTC; mutant reverse WPRE oIMR9103—
510 GGCATTAAAGCAGCGTATCC; mutant forward tdTomato oIMR9105—
511 CTGTTCCTGTACGGCATGG). UCN3-Cre heterozygous mice (strain Tg(Ucn3-cre)KF43Gsat/
512 Mmucd, MMRRC GENSAT) were crossbred with VGAT-Flpo heterozygous mice (Jax stock
513 #007909,B6.Cg-Slc32a1 2A-Flpo-D:Het) to obtain female double heterozygous UCN3-Cre::VGAT-
514 Flpo mice (Slc32a1 2A-Flpo-D:Het|Ucn3-Cre:Het|Rosa26<tomato>WT); genotyped using PCR for
515 the detection of heterozygosity (primers 5′- 3′: UCN3 Forward: CGAAGTCCCTCTCACACCTGGTT;
516 Cre Reverse: CGGCAAACGGAC-AGAAGCATT; Slc32a1 Mutant Forward: TGC ATC GCA TTG
517 TCT GAG TAG; Slc32a1 Mutant Reverse: GAC AGC CGT GAA CAG AAG G). Female mice, aged 8
518 to 10 weeks, weighing between 20 g and 25 g, were individually housed in ventilated cages sealed
519 with a HEPA-filter at 25 ± 1°C in a 12:12-hour light/dark cycle, lights on at 07:00 h. Vaginal smears
520 were performed when mice are 6 weeks old between 10:00 - 12:00 h daily. Only mice showing

521 regular estrous cycles were included. All animal procedures performed were approved by the King's
522 College London Animal Welfare and Ethical Review Body. Procedures were in accordance with UK
523 home office regulation.

524 **Stereotaxic injection of adeno-associated virus construct and fiber-optic or mini-endoscope**
525 **GRIN lens implantation**

526 All surgical procedures were carried out under general anesthesia using ketamine (Vetalar, 100
527 mg/kg, i.p.; Pfizer, Sandwich, UK) and xylazine (Rompun, 10 mg/kg, i.p.; Bayer, Leverkusen,
528 Germany) under aseptic conditions. Animals were secured in a David Kopf stereotaxic frame (Model
529 900, Kopf Instruments, CA, USA). Following bilateral ovariectomy, a midline incision was made in
530 the scalp to reveal the skull. Two small bone screws were inserted into the skull. A small hole was
531 drilled above the position of the MePD. The MePD coordinate (2.29 mm lateral, 1.60 mm posterior
532 from bregma, at a depth of 5.33 mm below the skull surface) was determined according to the
533 mouse brain atlas of Paxinos and Franklin[32]. A unilateral stereotaxic viral injection was performed to
534 target opsin or fluorescent protein expression in the MePD neurons, using a robot stereotaxic
535 system (Neurostar, Tubingen, Germany), with a 5-μL Hamilton microsyringe (Esslab, Essex, UK), at
536 the speed of 25 nl/min for 10 min.

537 Two transgenic animal models were used for LH blood sampling under optogenetic stimulation:
538 UCN3-Cre::VGAT-Flpo and VGAT-Cre-tdTomato. The following types of viral constructs were used
539 in separated cohorts of UCN3-Cre::VGAT-Flpo mice: (i) AAV-nEF-Con/Foff 2.0-ChRmine-oScarlet
540 (250 nl, 2.1×10^{12} gc/mL, Serotype:8, #137161, Addgene, Massachusetts, USA); (ii) AAV-nEF-
541 Con/Fon 2.0-ChRmine-oScarlet (250 nl, 1.9×10^{12} gc/mL, Serotype:8, # 137159, Addgene,
542 Massachusetts, USA); (iii) a mixture of AAV-nEF-Con/Foff 2.0-ChRmine-oScarlet (2.1×10^{12} gc/mL,
543 #137161) and pAAV-nEF-Coff/Fon-NpHR3.3-EYFP (1.9×10^{12} gc/mL; #137159, final volume 300 nl);
544 (iv) control virus AAV-Ef1a-DIO-EYFP (250 nl, 4.4×10^{12} gc/mL, Serotype:9, #27056, Addgene,
545 Massachusetts, USA). VGAT-Cre-tdTomato mice received unilateral injections of (i)
546 channelrhodopsin (ChR2) viral construct, (250 nl, 1.8×10^{12} gc/mL; Serotype:9; Addgene, #20298,

547 Massachusetts, USA) or (ii) control virus, AAV-Ef1a-DIO-EYFP (250 nl, 4.4 × 10^{12} gc/mL,
548 Serotype:9; Addgene, # 27056, Massachusetts, USA) into the MePD. Following injection, the needle
549 was kept in position for 10 min before going up slowly over 1 min. A unilateral fiber optic cannula
550 (200 μm, 0.39 NA, 1.25 mm ceramic ferrule; Doric Lenses, Quebec, Canada) was inserted into the
551 right MePD 0.15 mm above the injection site. After reaching the target, the fiber optic cannula was
552 secured on the skull using dental cement (Super-Bond Universal Kit, Prestige Dental, UK), bonded
553 to the screws and skull. Finally, the incision in the scalp was closed with suture. Animals were given
554 1 week to recover, after which they were handled 20 min daily to acclimatize to experimental
555 procedures for a further 2 weeks.

556 For mini-endoscope *in vivo* calcium imaging, only UCN3-Cre::VGAT-Flpo transgenic animals were
557 used. Separate mice cohorts received the following viral injection into the MePD: (i) a mixture of
558 pAAV-Syn-Flex-rc[Chrimson-tdTomato] (2.0×10^{12} gc/mL, Serotype:5, #62723, Addgene,
559 Massachusetts, USA) + pAAV-EF1a-fDIO-GCaMP6s (2.3×10^{12} gc/mL; Serotype:8; #105715,
560 Addgene, Massachusetts, USA; final volume 400 nl); (ii) a mixture of pAAV-Syn-Flex-rc[Chrimson-
561 tdTomato] (2.0×10^{12} gc/mL, Serotype:5, #62723, Addgene, Massachusetts, USA) +
562 pAAV.CAG.Flex.GCaMP6s.WPRE.SV40 (4.3×10^{12} gc/mL; Serotype:9; # 100842, Addgene,
563 Massachusetts, USA; final volume 400 nl); (iii) a mixture of control virus pAAV-hSyn-DIO-mCherry
564 (2.3×10^{12} gc/mL, Serotype:9, #50459) + pAAV-EF1a-fDIO-GCaMP6s (2.3×10^{12} gc/mL, Serotype:8,
565 #105715, final volume 400nl) . One week after administering the virus, a 600-μm diameter, 7.2-mm
566 long gradient index (GRIN) ProView™ Integrated Lens (Inscopix, PN:100-004554) was implanted at
567 the same location as the viral injection. The surface of the skull was scored, using the tip of a
568 surgical scalpel, and four screws were inserted into the skull. This was done to enhance the
569 adhesion of dental cement to the skull, thereby reducing the interference of movement on *in vivo*
570 recording. Before insertion of the GRIN lens, a 23 G needle was slowly lowered at a speed of 5.0
571 mm/min into the brain (2.42 mm lateral, 1.52 mm posterior from bregma, depth of 5.05 mm below
572 the skull surface) to make a needle track to facilitate the insertion of the GRIN lens without causing
573 brain distortion along its route. The GRIN lens was then inserted into the brain at a rate of 0.6

574 mm/min, using the same coordinates as the needle precutting. To secure the GRIN lens with
575 integrated baseplate in position, we used a light curing adhesive (iBond Universal, Kulzer GmbH,
576 Leipziger, Germany) along with a cured radiopaque hybrid dental cement (Gradia Direct Flo, GC
577 corporation, Tokyo, Japan), bonding it to the head screws and skull. A GRIN lens baseplate dust
578 cover (Inscopix) was rescued in place to protect the lens. After 4 weeks the mice were re-
579 anaesthetized as described above and underwent bilateral ovariectomy.

580 **Serial blood sampling for LH measurement**

581 The mouse's tail-tip was excised using a sterile scalpel. Then the chronically unilaterally implanted
582 fiber optic cannula was connected to a multimode fiber optic rotary joint patch cables (Thorlabs Ltd,
583 Ely, UK) via a ceramic mating sleeve to allow the animal freedom of movement. Mice were left for 1
584 h to habituate. A Grass SD9B stimulator-controlled DPSS laser (Laserglow Technologies, Toronto,
585 Canada) was utilized to deliver either green light (532 nm wavelength, 10 Hz, 5 seconds on 5
586 seconds off, 10 mW, 10-ms pulse width,) or blue light (473 nm wavelength, 5 Hz, 5 seconds on 5
587 seconds off, 5 mW, 10-ms pulse width,). The light pattern was controlled using software designed in
588 house. After 1 h of acclimatization, serial blood samples (5-μL) for LH pulse measurement were
589 collected every 5 min for 2 h between 10:00 - 12:00 h: 0-60 min for control blood sampling period,
590 and 60-120 min under stimulation or equivalent no-stimulation control period. Blood samples were
591 diluted in 45 μL of Phosphate-Buffered Saline (PBS) containing 0.2% Bovine Serum Albumin (BSA)
592 and 0.05% Tween-20 (PBST) and immediately placed on dry ice and stored at −80°C until later
593 analysis.

594 **LH assay**

595 LH measurement was performed using an LH ELISA assay as reported previously[33]. A mouse LH
596 standard (mLH; AFP-5306A, NIDDK-NHPP, USA) was used to establish a standard curve for the
597 quantitative measurement. The following antibodies were used in the assay: (i) coating antibody
598 (RRID: AB_2665514, monoclonal antibovine LH beta subunit antiserum, 518B7, University of
599 California, CA, USA); (ii) anti-LH antibody (RRID: AB_2665533; National Hormone & Peptide

600 Program, CA, USA); (iii) secondary antibody (RRID: AB_772206, GE Healthcare, Chicago, Illinois,
601 USA). The inter-assay and intra-assay variations were 10.53% and 5.74%, respectively. The assay
602 sensitivity was 0.023 ng/mL.

603 **LH pulse statistical analysis**

604 LH pulses were verified using the Dynpeak algorithm in Scilab 5.5.2 programme[34]. The Dynpeak
605 algorithms were classified for OVX mice based on previously established parameters[35]. The average
606 LH inter-pulse interval was calculated for the 1-h control period and the 1-h stimulation period in both
607 experimental and control mice. Statistical significance was assessed using a 2-way ANOVA unless
608 otherwise stated. Data was represented as mean ± SEM and $p<0.05$ was considered significant.

609 **Mini-endoscope-based Calcium imaging**

610 **Under optogenetic stimulation of MePD UCN3 neurons.** Prior to recording, animals were
611 handled daily for 5 to 6 weeks to get accustomed to the experimental setup. The Data Acquisition
612 (DAQ) box (Inscopix, PN:100-005904) was turned on and connected to the computer wirelessly.
613 The Data Acquisition Software (IDAS; Inscopix, Inc.) was accessed through the Chrome web
614 browser on the computer communicating with the DAQ box. Adequate DAQ box storage capacity
615 was checked routinely before Calcium imaging. The GRIN lens baseplate dust cover was gently
616 removed from the mouse's head, after which the minscope camera was secured to the baseplate
617 platform. Equipped with the head-mount miniscope (nVoke2, Inscopix, SN: BB-11238601), the
618 mouse was then placed back into its home cage. The optimal focal plane was chosen by adjusting
619 the lens focus to achieve clear cell morphology. The exposure time was fixed at 50 ms. The frame
620 rate was set to 20 Hz. Subsequently, gain, and LED power were optimized based on image
621 histograms before initiating recording. Two types of LED were used during the recording: (i) EX-LED
622 (0.2-0.4 mW, 435-460 nm excitation filter) for GCaMP6s signal detection in the GABA or UCN3
623 neurons; (ii) OG-LED (10 mW, 590-650 nm excitation filter) for Chrimson optogenetic stimulation of
624 the UCN3 neurons. After the mice were attached to the miniscope, they were given 1-2 h for
625 adaptation. For stimulation of the UCN3 neurons, the OG-LED was set to 10 Hz, 5 seconds on 5

626 seconds off, and a 10-ms pulse width. Once the animals had acclimatized, the GCaMP6s recording
627 of the GABA neurons or UCN3 neurons was started with a protocol of 2 min baseline before
628 stimulation for 2 min. Optogenetic stimulation was randomized for the 10 Hz, with a 5-min interval
629 between each to prevent photobleaching of GCaMP6s. Once the experiment was concluded, the
630 miniscope was gently detached, and the baseplate cover was reattached and secured with its
631 screw. The recordings were performed between 9:00 h and 15:00 h. Three groups of animals were
632 included in this experiment: (i) mice with UCN3 neurons expressing opsin and GABA neurons
633 expressing GCaMP; (ii) mice with UCN3 neurons expressing both opsin and GCaMP, serving as a
634 positive control; (iii) mice with UCN3 neurons expressing mCherry and GABA neurons expressing
635 GCaMP, serving as a negative control.

636 **Under restraint stress.** The system was set up and the mouse was connected to the miniscope as
637 described above but with the OG-LED turned off. Once the mouse had settled, the experiment
638 started with a 3 min baseline recording, followed by 3 min of recording under hand-held restraint.
639 Finally, the miniscope was detached and the baseplate cover was reattached. The experiments were
640 performed between 9:00 h and 15:00 h. The animals in this experiment were the same as those
641 used in the optogenetic stimulation protocol described above but were divided into two groups
642 depending on whether GCaMP was expressed in the UCN3 or GABA neurons, regardless of
643 whether opsin or mCherry was expressed in the UCN3 cells.

644 ***In vivo* calcium imaging recording processing**

645 The video data, with a resolution of 1280 pixels x 800 pixels, was exported from the DAQ box
646 through the file manager to a desktop computer and processed with the Inscopix Data Processing
647 Software (IDPS). Within the IDPS, there are six essential steps for extracting single-cell calcium
648 transient data from the recorded video: down-sampling, cropping, spatial filtering, motion correction,
649 trace normalization (ΔF/F), and cell identification. First, the video underwent both spatial down-
650 sampling and temporal down-sampling by a factor of 2 and was cropped to enhance processing
651 speed, focusing on the region of interest where the GCaMP signal was observed. Spatial filtering,

652 with a threshold ranging between 0.005 (low) and 0.5 (high) was used to distinguish individual pixels
653 in the video image, creating a high-contrast image. A mean intensity projection image was
654 generated. Motion correction was subsequently conducted, using the mean intensity projection
655 image as a reference. Motion correction was applied again using one of the frames affected by
656 movement while simultaneously drawing a region of interest (ROI) where UCN3 accumulates to
657 enhance the effectiveness of motion correction. For the recordings with GCaMP signals from GABA
658 neurons, we did not use the built-in motion correction function of IDPS. Instead, we used the
659 MATLAB (version R2022a) implementation of the open-source algorithm NoRMCorre[36] with default
660 parameters for both rigid and non-rigid (patch size 64 pixels and overlap 32) motion correction as
661 long as a minimum correlation of the frames with the mean frame above 0.8 is achieved.
662 Occasionally, if the minimum correlation is not met, an extra step of non-rigid motion correction with
663 coarser patches is applied. This is performed by doubling the patch size and their overlap to 128 and
664 64, respectively. Corrected videos were saved in TIFF format for further analysis via IDPS. Following
665 motion correction, pixel intensity, $F(x,y)$, in each frame of the movie was normalised using the
666 following formula $\frac{(F(x,y) - F_{baseline}(x,y))}{F_{baseline}(x,y)}$, where $F_{baseline}(x,y)$ is the baseline pixel intensity calculated
667 by taking the mean value of the pixel across the entire movie. Finally, regions of interest were
668 identified automatically using the cell identification algorithm provided by IDPS, based on principal
669 component and independent component analysis (PCA-ICA algorithm).

670 **Validation of virus injection, fiber optic cannula and GRIN lens implantation**

671 Once the experimental procedures were completed, a lethal dose of ketamine was used to
672 humanely euthanize the mice. The mice were perfused transcardially with heparinized saline (5
673 U/ml) for 5 min, followed by ice-cold 4% paraformaldehyde (PFA) for 15 min using a pump
674 (Minipuls,156 Gilson, Villiers Le Bel, France). The brains were collected and post-fixed sequentially
675 at 4°C in a solution of 15% sucrose in 4% PFA and later in a solution of 30% sucrose in phosphate
676 buffer until they sank. They were then snap frozen on dry ice and stored in -80°C until processing.
677 The brains were coronally sectioned (30 µm) between +0.5 mm and -2.7 mm from the bregma using

678 a cryostat (Bright Instrument Co., Huntingdon, UK), and sections were mounted on microscope
679 slides, air-dried, and covered with slips using Prolonged Antifade mounting medium (Molecular
680 Probes, Inc. OR, USA). The accuracy of injection sites, fiber optic cannula and GRIN lens
681 implantation were confirmed by Axioskop 2 Plus microscope equipped with AXIOVISION 4.7
682 (Zeiss). Images were captured using Axioskop 2 Plus microscope (Carl Zeiss). Only the data of
683 mice with correct viral infection and implantation of cannula and lens in the MePD were included in
684 the analysis.

685 **Immunohistochemistry**

686 To assess the targeting of viral labeling to UCN3 neurons in the MePD, we used the indirect
687 immunofluorescence technique to localize UCN3 neurons. Every 4th section from each brain was
688 washed in potassium phosphate-buffered saline (KPBS) and incubated in blocking solution (KPBS
689 containing 1% BSA, 0.03% Triton X-100 and 5mg/ml heparin) at room temperature for 1 hour
690 followed by incubated in a rabbit polyclonal anti-UCN3 antibody (1:2000 dilution)[37] in the blocking
691 solution (Code: PBL 7218, kindly provided by J. Vaughan, Salk Institute, La Jolla, CA, USA) for 48
692 hours at 4°C. The brain sections were then processed with goat anti-rabbit IgG (H + L), a
693 biotinylated secondary antibody (1:1000 dilution; Cat. No. BA-1000, Vector Laboratories,
694 Burlingame, CA, USA) overnight at 4°C. After rinses in KPBS, visualization of UCN3 immunoactivity
695 was achieved using Streptavidin, Alexa Fluor 405 conjugate (1:200 dilution; Cat. No. S 32351,
696 Thermo Fisher Scientific, Waltham, MA, USA) for 2 hours at room temperature. The sections were
697 finally washed, mounted onto slides and cover slipped. Omission of the UCN primary antibody and
698 its pre-incubation resulted in the absence of specific staining. Brain sections from each experimental
699 group were processed on the same day to control for inter-batch variability. To preserve the
700 fluorescence of the virally expressed proteins, all subsequent steps were performed in a dark box.
701 Semiquantitative analysis of immunostaining data was carried out on AxioVision microscope image
702 system. UCN3-positive neurons were identified by Alexa Fluor 405 fluorescence, while native
703 fluorescence (e.g. tdTomato or oScarlet) was used for virus-transduced neurons identification. The
704 number of virus-labeled, UCN3-immunoreactive cells and co-localized cells in the MePD were

705 quantified on 4 sections from each mouse brain. Targeting efficiency was defined as the percentage
706 of virus-labeled cells that were also positive for UCN3.

707 **Data analysis**

708 The data processing protocol we employ in this study was performed in two phases: pre-intervention
709 and intervention (either via optogenetic stimulation or restraint stress). For our analysis, we use the
710 smoothed deconvolved traces generated by the OASIS method[38], which improves the signal-to-
711 noise ratio (SNR) and mitigates noise interference. All traces are rescaled between 0 and 1 (min-
712 max normalization), and then further normalized to mean zero and unit variance. The analysis
713 process is divided into three key steps: i) identification of GABA cells co-expressing UCN3 and
714 removing them from further analysis; ii) estimating and comparing functional connectivity before and
715 during intervention; iii) clustering analysis based on pairwise association-derived dissimilarity scores.

716 In step (i), we use power spectral density (PSD) analysis and K-means clustering (using Euclidean
717 distance) to identify GABA neurons with activity that mimics the pattern of optic stimulation, evidence
718 that they are co-expressing UCN3.

719 **PSD filtering.** For each trace, we compute the PSD during the stimulation phase. Cells with PSD
720 values at 0.1 Hz (the frequency of the stimulus 5 seconds on and 5 seconds off cycle) above 0.37
721 Hz^{-1} are labelled as co-expressing UCN3. This threshold is determined from recordings of UCN3
722 cells under optic stimulation, by calculating the median of the minimum PSD values at 0.1 Hz from
723 each dataset (see Supplementary Fig. 2**B**).

724 **K-means clustering.** Using the Euclidean distance metric, we cluster the traces during the
725 stimulation phase into two groups, aiming to separate neurons into GABA-only neurons and neurons
726 co-expressing UCN3 and GABA. Clustering separated a small group of neurons with activity
727 mimicking the optic stimulation oscillatory pattern (see Supplementary Fig. 2**C**). Recordings of MePD
728 UCN3 neurons shows that under optogenetic stimulation their activity rises and declines in phase
729 with on and off periods of stimulation (shown in Fig. 3**A**); therefore, this small number of cells was
730 labelled as co-expressing UCN3.

731 The union of neurons identified by either method as co-expressing UCN3 and GABA are excluded
732 from further analysis. By applying both filters, we aim to robustly identify purely GABA-expressing
733 neurons. We acknowledge the possibility that some cells may pass through the filters or that a few
734 purely GABA-expressing neurons may be inadvertently excluded. However, our dual approach of
735 employing power spectral density (PSD) analysis and K-means clustering minimizes this possibility
736 and is essential to ensure our analysis remains focused exclusively on GABA-expressing neurons.
737 Nevertheless, we take a further step and visually inspect the calcium recording traces for any
738 potential anomalies such as regular oscillations in-phase with the stimulation and/or massive
739 increase in calcium level during the intervention period. Any identified anomalies of this sort are also
740 dropped from data sets.

741 **Comparing pre-intervention and intervention cell-cell interaction strength**

742 Following step (i), the remaining dataset contains only traces associated with GABA neurons, which
743 are not directly activated by our optic stimulation protocol. In step (ii), we assess the functional
744 connectivity between the observed neurons using Pearson's correlation[39] defined as

745 $$corr(x,y) = \frac{R(x,y)}{\sqrt{R(x,x)R(y,y)}},$$

746 where $R(x,y) = \sum_{i=1}^{N}(x_i - \bar{x})(y_i - \bar{y})$ represents cross-correlation with N as the length of x and y.

747 Using the above measures, we construct the corresponding cross-correlation matrices (see for an
748 example Fig. 1**H&I**).

749 To evaluate changes in pairwise cell interactions between the pre-intervention and intervention
750 phases, we compute the pairwise Riemannian distance[40] between correlation matrices from pre-
751 intervention and intervention episodes. The Riemannian distance here is defined as

752 $$d(A, B) = \left(\sum_i ln(\lambda_i)^2\right)^{1/2}$$

where ln is the natural logarithm and λ_i indicates the joint eigenvalues of symmetric positive definite (SPD) cross-correlation matrices A and B. The size of the matrices directly affects the riemannian distance such that the distance among matrices increases as the size increases. With a good approximation square root describes this relationship. However, we take a more accurate approach and normalize all the Riemannian distances by the mean pairwise Riemannian distance between many SPD matrices generated randomly. To make sure that the random generation of correlation matrices is uniform, we employ the Metropolis-Hasting method introduced in[41]. Normalizing the Riemannian distances guarantees that the distance is not influenced by matrix size.

Clustering analysis

In step (iii), we apply agglomerative hierarchical clustering (using the average linkage criterion; scikit-learn package in Python™) to classify cells based on the dissimilarity of their calcium activity, given as

$$D(x, y) = 1 - corr(x,y).$$

To determine the optimal number of clusters and robustness of clustering, we employed a bootstrapping technique. This involved resampling (without replacement) 75% of the cells and clustering the resulting dataset with different numbers of clusters (2, 3, and 4) using hierarchical or K-means clustering with either the covariance or corr as the dissimilarity measure. This resampling process was repeated 100 times.

For each resample dataset, we evaluate the clustering performance, using the Silhouette Coefficient (SC)[42] which measures the cohesion within clusters and their separation, with values ranging from -1 (poor performance) to 1 (good performance). Results of the evaluation are given in Supplementary Figs. 4-6, showing that the Silhouette Coefficient is significantly higher for 2 clusters compared to 3 or 4 clusters in the case of both hierarchical and K-means clustering.

776 **Modeling**

777 We build on our previously published modelling framework of MePD circuit[11] by incorporating
778 dynamic stimulation by UCN3 as observed experimentally (as shown in Fig. 3). To this end we
779 define UCN3 input into the populations of glutamatergic neurons and GABA interneurons with a
780 strength given by the parameter γ. The activity of UCN3 during stimulation is approximated via
781 sinusoidal function:

782 $$U_{stim}(t) = \gamma B + Asinsin\ (2\pi f t)\ ,$$

783 where B and A are the baseline UCN3 activity and the amplitude, respectively, while the parameter
784 f is the frequency of the sigmoid wave. We approximate UCN3 activity during restraint stress using
785 two exponential functions:

786 $$U_{stress}(t) = \gamma(atexp\ (-r_2 t) + b(1 - exp\ (-r_1 t)\ )\ ),$$

787 where the function initially increases with magnitude a then decreases to a plateau value given by
788 the parameter b. The parameters r_1 and r_2 are responsible for the rate of increase of the first term
789 and rate of decrease to a plateau in the second term.

790 Briefly, the model captures the dynamics of the MePD intracellular calcium activity of three
791 populations: glutamatergic neuronal population (excitatory) and the populations of GABA
792 interneurons and GABA efferent neurons (inhibitory). We build on our previous work[11] by assuming
793 that excitatory (UCN3) input is provided to the populations of GABA interneurons and glutamate (Fig
794 3). Previous analysis of the model indicated that negative feedback between GABA and
795 glutamatergic neuronal populations as well as glutamatergic self-excitation are critical mechanisms
796 for inducing oscillatory dynamics[11]. However, providing glutamatergic inputs to both populations of
797 GABA neurons result in a null phase difference between the populations. Therefore, we opted to
798 provide glutamatergic input only to the population of GABA efferent neurons.

799 To investigate how the amygdala modulates the activity in the GnRH pulse generator, we couple the
800 above-described MePD model to our KNDy network model, where the oscillatory dynamics of the

801 KNDy acts as a proxy of LH pulsatility[25]. Here we couple the model via providing only inhibitory
802 output from MePD GABA efferent neurons population to KNDy, as it was previously shown that
803 glutamate plays a modulatory role to the MePD output rather than directly affecting the KNDy
804 network[11]. We then calibrate the coupled by reproducing the experimental results from Ivanova et
805 al.[23] (Supplementary Fig. 8). Further modeling details, such as equations governing model
806 dynamics and model parameter values, can be found in Supplementary Information. The simulations
807 have been done in MATLAB (version R2023b).

808 Data Availability

809 Source data are provided with this paper. Further information that supports the findings of this study
810 is available from the corresponding authors upon request.

811 Code Availability

812 The code for reproducing the data analysis (Python™), mathematical modeling (MATLAB), and
813 figure generation for both the main text and Supplementary information, along with a test dataset, is
814 publicly available at: https://github.com/mv-kr/MePD_GABA.

815 References

816 1. Yeo, S.-H., Kyle, V., Blouet, C., Jones, S. & Colledge, W. H. Mapping neuronal inputs to Kiss1
817 neurons in the arcuate nucleus of the mouse. *PLOS ONE* **14**, e0213927 (2019).

818 2. Moore, A. M., Coolen, L. M. & Lehman, M. N. Kisspeptin/Neurokinin B/Dynorphin (KNDy) cells
819 as integrators of diverse internal and external cues: evidence from viral-based monosynaptic
820 tract-tracing in mice. *Sci. Rep.* **9**, 14768 (2019).

821 3. Li, X. F. & O'Byrne, K. T. Stress and the Reproductive System. in *Knobil and Neill's Physiology*
822 *of Reproduction: Two-Volume Set* vol. 2 1637–1660 (ELSEVIER SCIENCE INC, 2014).

823 4. Yu, J., Li, X.-F., Tsaneva-Atanasova, K., Zavala, E. & O'Byrne, K. T. Chemogenetic activation of
824 PVN CRH neurons disrupts the estrous cycle and LH dynamics in female mice. *Front.*
825 *Endocrinol.* **14**, 1322662 (2023).

826 5. Kreisman, M. J., Tadrousse, K. S., McCosh, R. B. & Breen, K. M. Neuroendocrine Basis for
827 Disrupted Ovarian Cyclicity in Female Mice During Chronic Undernutrition. *Endocrinology* **162**,
828 bqab103 (2021).

829 6. Bethea, C. L., Centeno, M. L. & Cameron, J. L. Neurobiology of Stress-Induced Reproductive
830 Dysfunction in Female Macaques. *Mol. Neurobiol.* **38**, 199–230 (2008).

831 7. Herod, S. M., Pohl, C. R. & Cameron, J. L. Treatment with a CRH-R1 antagonist prevents
832 stress-induced suppression of the central neural drive to the reproductive axis in female
833 macaques. *Am. J. Physiol. Endocrinol. Metab.* **300**, E19-27 (2011).

834 8. Nair, B. B. *et al.* Impact of chronic variable stress on neuroendocrine hypothalamus and pituitary
835 in male and female C57BL/6J mice. *J. Neuroendocrinol.* **33**, e12972 (2021).

836 9. Comninos, A. N. *et al.* Kisspeptin signaling in the amygdala modulates reproductive hormone
837 secretion. *Brain Struct. Funct.* **221**, 2035–2047 (2016).

838 10. Lass, G. *et al.* Optogenetic stimulation of kisspeptin neurones within the posterodorsal medial
839 amygdala increases luteinising hormone pulse frequency in female mice. *J. Neuroendocrinol.*
840 **32**, e12823 (2020).

841 11. Nechyporenko, K. *et al.* Neuronal network dynamics in the posterodorsal amygdala: shaping
842 reproductive hormone pulsatility. *J. R. Soc. Interface* **21**, 20240143 (2024).

843 12. Adekunbi, D. A. *et al.* Role of amygdala kisspeptin in pubertal timing in female rats. *PLoS ONE*
844 **12**, e0183596 (2017).

845 13. Ivanova, D. *et al.* Role of Posterodorsal Medial Amygdala Urocortin-3 in Pubertal Timing in
846 Female Mice. *Front. Endocrinol.* **13**, (2022).

847 14. Adekunbi, D. A. *et al.* Kisspeptin neurones in the posterodorsal medial amygdala modulate
848 sexual partner preference and anxiety in male mice. *J. Neuroendocrinol.* **30**, e12572 (2018).

849 15. Wu, Y. E. *et al.* Neural control of affiliative touch in prosocial interaction. *Nature* **599**, 262–267
850 (2021).

851 16. Ivanova, D. *et al.* Urocortin3 in the Posterodorsal Medial Amygdala Mediates Stress-induced
852 Suppression of LH Pulsatility in Female Mice. *Endocrinology* **162**, 1–14 (2021).

853 17. McIntyre, C. *et al.* GABA Signaling in the Posterodorsal Medial Amygdala Mediates Stress-
854 induced Suppression of LH Pulsatility in Female Mice. *Endocrinology* **164**, 1–11 (2023).

855 18. Keshavarzi, S., Sullivan, R. K. P., Ianno, D. J. & Sah, P. Functional Properties and Projections
856 of Neurons in the Medial Amygdala. *J. Neurosci.* **34**, 8699–8715 (2014).

857 19. Choi, G. B. *et al.* Lhx6 delineates a pathway mediating innate reproductive behaviors from the
858 amygdala to the hypothalamus. *Neuron* **46**, 647–660 (2005).

859 20. Bian, X. Physiological and morphological characterization of GABAergic neurons in the medial
860 amygdala. *Brain Res.* **1509**, 8–19 (2013).

861 21. Lewis, K. *et al.* Identification of urocortin III, an additional member of the corticotropin-releasing
862 factor (CRF) family with high affinity for the CRF2 receptor. *Proc. Natl. Acad. Sci. U. S. A.* **98**,
863 7570–7575 (2001).

864 22. Shemesh, Y. *et al.* Ucn3 and CRF-R2 in the medial amygdala regulate complex social
865 dynamics. *Nat. Neurosci.* **19**, 1489–1496 (2016).

866 23. Ivanova, D., Li, X.-F., McIntyre, C. & O'Byrne, K. T. Posterodorsal Medial Amygdala Urocortin-3,
867 GABA, and Glutamate Mediate Suppression of LH Pulsatility in Female Mice. *Endocrinology*
868 **164**, 1–13 (2023).

869 24. Yuste, R., Cossart, R. & Yaksi, E. Neuronal ensembles: Building blocks of neural circuits.
870 *Neuron* **112**, 875–892 (2024).

871 25. Voliotis, M. *et al.* The Origin of GnRH Pulse Generation: An Integrative Mathematical-
872 Experimental Approach. *J. Neurosci.* **39**, 9738–9747 (2019).

873 26. Hochgerner, H. *et al.* Neuronal types in the mouse amygdala and their transcriptional response
874 to fear conditioning. *Nat. Neurosci.* **26**, 2237–2249 (2023).

875 27. Li, Y. *et al.* Neuronal Representation of Social Information in the Medial Amygdala of Awake
876 Behaving Mice. *Cell* **171**, 1176-1190.e17 (2017).

877 28. Pardo-Bellver, C., Cádiz-Moretti, B., Novejarque, A., Martínez-García, F. & Lanuza, E.
878 Differential efferent projections of the anterior, posteroventral, and posterodorsal subdivisions of
879 the medial amygdala in mice. *Front. Neuroanat.* **6**, 33 (2012).

880 29. Polepalli, J. S., Gooch, H. & Sah, P. Diversity of interneurons in the lateral and basal amygdala.
881 *Npj Sci. Learn.* **5**, 10 (2020).

882 30. Patel, A. H. *et al.* Kisspeptin in functional hypothalamic amenorrhea: Pathophysiology and
883 therapeutic potential. *Ann. N. Y. Acad. Sci.* **1540**, 21–46 (2024).

884 31. Barbagallo, F. *et al.* Gene-environment interaction in functional hypothalamic amenorrhea.
885 *Front. Endocrinol.* **15**, 1423898 (2024).

886 32. Paxinos, G. & Franklin, K. B. J. *Paxinos and Franklin's the Mouse Brain in Stereotaxic*
887 *Coordinates*. (2019).

888 33. Steyn, F. J. *et al.* Development of a Methodology for and Assessment of Pulsatile Luteinizing
889 Hormone Secretion in Juvenile and Adult Male Mice. *Endocrinology* **154**, 4939–4945 (2013).

890 34. Vidal, A., Zhang, Q., Médigue, C., Fabre, S. & Clément, F. DynPeak: An Algorithm for Pulse
891 Detection and Frequency Analysis in Hormonal Time Series. *PLOS ONE* **7**, e39001 (2012).

892 35. Yang, J. A. *et al.* Acute Psychosocial Stress Inhibits LH Pulsatility and Kiss1 Neuronal Activation
893 in Female Mice. *Endocrinology* **158**, 3716–3723 (2017).

36. Pnevmatikakis, E. A. & Giovannucci, A. NoRMCorre: An online algorithm for piecewise rigid motion correction of calcium imaging data. *J. Neurosci. Methods* **291**, 83–94 (2017).

37. Battagello, D. S. *et al.* Anatomical Organization of Urocortin 3-Synthesizing Neurons and Immunoreactive Terminals in the Central Nervous System of Non-Human Primates [Sapajus spp.]. *Front. Neuroanat.* **11**, (2017).

38. Friedrich, J., Zhou, P. & Paninski, L. Fast online deconvolution of calcium imaging data. *PLOS Comput. Biol.* **13**, (2017).

Acknowledgements

We thank Ms Sumi Mathew for her technical support with genotyping mice.

S.F., M.V., K.T.A., K.T.O., X.F.L. gratefully acknowledge the financial support of BBSRC via grants BB/W005913/1 (KCL), BB/W005883/1 (Exeter) and BB/S019979/1. KTA gratefully acknowledges the financial support of the EPSRC via grant EP/T017856/.

Contributions

J.Y. contributed data acquisition and data analysis, S.F. contributed data analysis, K.N. contributed modeling, M.V. contributed managing data analysis, X.F.L. contributed managing data acquisition, H.Y. contributed data acquisition, Y.L. contributed data acquisition, J.Y. contributed data acquisition, O.H. contributed data acquisition, R.D.B. contributed data acquisition, B.S. contributed data acquisition, K.T.O., K.T.A. and M.V. contributed to managing the project. All authors contributed to writing the manuscript.

Competing interests

The authors declare no competing interests.

Corresponding author

Correspondence and requests for materials should be addressed to Krasimira Tsaneva-Atanasova (K.Tsaneva-Atanasova@exeter.ac.uk), Kevin T. O'Byrne (kevin.o'byrne@kcl.ac.uk), Margaritis Voliotis (m.voliotis@exeter.ac.uk).

Open Access

For the purpose of open access, the authors have applied a 'Creative Commons Attribution (CC BY) licence to any Author Accepted Manuscript version arising from this submission.